Avionic Piezoelectric Deicing System: Numerical and Experimental Investigation of the Use of Extension Modes for Deicing

Modar Jomaa, Pierre-Etienne Lévy, Dejan Vasic, François Costa, Marwan Ali

Avionic Piezoelectric Deicing System: Numerical and Experimental Investigation of the Use of Extension Modes for Deicing

Modar JOMAA[1,4], Pierre-Etienne LÉVY[1], Dejan VASIC[2], François COSTA[3] and Marwan ALI[4]
[1]Université Paris-Saclay, ENS Paris-Saclay, CNRS, SATIE, 91190 Gif-sur-Yvette, France
[2]Université de Cergy-Pontoise, 95031 Cergy-Pontoise, France
[3]Université Paris Est Créteil, INSPE, 94000 Créteil, France
[4]Safran Tech, groupe de recherche E&E, 78117 Magny-Les-Hameaux, France

Abstract
A proof of the concept of utilizing lightweight piezoelectric actuators for deicing aircraft's leading edges with minimal power needs is proposed. This type of deicing applies vibration to the structure by activating its own resonant frequencies to generate sufficient stress to break the ice and detach it from the substrate. The deicing mechanism depends strongly on the chosen excitation mode, whether it's flexural (bending) mode, extension (stretching) mode, or a combination in between, hence affecting the efficiency and effectiveness of the deicing process. Using extensional modes generates shear stresses at the interface leading edge/ice great enough to delaminate the ice. Deicing was demonstrated with a power input density of 0.074 W/cm² and a surface ratio of 0.07 piezoelectric actuators per cm². First, a numerical method for positioning piezoelectric actuators and choosing the proper resonance mode was validated to assist in the system's design. Then, the numerical method was used to implement piezoelectric deicing on a more representative structure of an aircraft wing or nacelle. Finally, a converter topology adapted for deicing application was proposed.

Introduction

An ultrasound piezoelectric system is used in a wide range of applications where efficient and economical energy conversion is required. Some of the industrial applications for which an ultrasound piezoelectric system can be used are water purification, ultrasonic cleaning and welding. A new application of piezoelectric actuators is the avionic deicing system.
The aircraft industry is undergoing a significant transformation with a notable shift towards a "More Electric Aircraft" (MEA). This transition is driven by various factors, including environmental concerns, technological advancements, and the need for improved efficiency and performance. We are therefore witnessing a gradual increase in the role of electrical energy in onboard applications. This electrification trend aims to replace all non-propulsive systems (hydraulic and pneumatic) with electromechanical alternatives in order to optimize aircraft performance, decrease operating and maintenance costs, increase dispatch reliability, and reduce gas emissions. Among the systems targeted by this transition is the deicing system.
Since ice accretion on aircraft wings and nacelles can significantly impact aerodynamic efficiency and balance, resulting in reduced lift and increased drag, aircraft require an ice protection system capable of meeting the demands of various certifications for full-icing clearance. A variety of deicing methods that defer by, the energy used, are employed today to prevent ice formation. These include: turbine engine bleed air, pneumatic deicing boot system, chemical fluid, and electrically heated systems [1]. However, these methods are classified as very energy-consuming and are only suitable for some aircraft categories. Concerning electromechanical technologies such as electro-impulsive [2], electro-expulsive [3], and piezoelectric [4], the latter stands out as the most promising solution in terms of power consumption, weight, and cost effectiveness.
This paper aims to produce a numerical model of a piezoelectric system in order to investigate crucial design parameters such as actuator positioning and sequencing, and then validate it through an experimental setup. A converter topology adapted to piezoelectric actuators for deicing applications was selected and developed to drive the deicing system.

1. PIEZOELECTRIC DEICING SYSTEM

The operating principle of deicing systems based on piezoelectric actuators is to apply microscopic vibrations at a specific frequency to the structure to

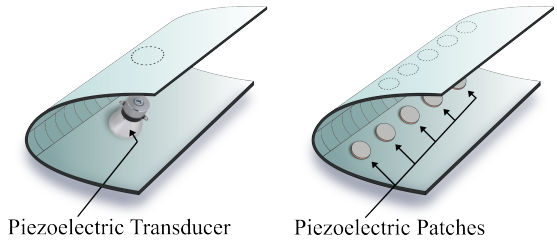

Fig. 1 Configuration of a piezoelectric de-icing system with piezoelectric patches and transducers.

delaminate and crack the ice. Depending on the resonance mode, these electromechanical vibrations produce a stress field that initiates cohesive fractures in the ice, adhesive fracture at the interface leading edge/ice, or both [5]. Two configurations were introduced in the literature for using piezoelectric actuators. The first configuration with the Langevin transducer was used for its ease of installation using bolts, and the lower risk of mechanical failure due to their prestressed structure which allows them to withstand higher stresses during operation. However, the utilization of prestressed PZT ceramics, mainly designed to stimulate structural flexural modes, can, in the best cases result in some ice delamination [6]. This issue, coupled with their substantial weight, make them less advantageous. The second configuration with piezoelectric patches which can be glued to the mechanical structure was the most commonly tested in the literature and seemed to be more promising (Fig. 1).

1.1. Ice properties & Fracture mechanisms

In the proposed deicing method, knowledge of the ice properties is critical. Many investigations and experiments have been conducted to assess the adhesive and cohesive strength of ice on diverse materials and in various icing conditions [7], [8]–[13]. These studies revealed that the expected adhesive shear strength value of refrigerated glaze ice can be estimated to be between 0.24 MPa and 1.7 MPa. The average adhesion shear strength of freezer ice to steel at -10°C was experimentally measured to be 1.5 MPa and the maximum was found to be at 1.66 MPa [14] while the cohesive tensile strength was found to be between [0.6 – 3] MPa [15]–[17]. Glaze ice characteristics are listed in TABLE I.

TABLE I

GLAZE ICE CHARACTERIZATION

Glaze ice	
Young's modulus (E)	9.3 GPa
Poisson's ratio (υ)	0.325
Density (ρ)	900 kg/m^3
Cohesive strength	[0.6 - 3] MPa
Adhesive strength	[0.24 – 1.7] MPa

In [18], fractures mechanisms were stated. The first mechanism starts when tensile stress exceeds ice tensile strength leading to a cohesive fracture at the top of the ice layer which then propagates through the ice until the bottom at the ice/substrate interface. Consequently, adhesive fractures occur at this point, leading to ice delamination (Fig. 2). Cohesive fractures alone are insufficient for deicing as ice can stick to the surface on which it is accreted. Therefore, they should always be coupled with adhesive fractures to allow ice debonding. The second mechanism starts when shear stress exceeds the ice/substrate interface shear strength leading to the initiation of an adhesive fracture and then the propagation of this adhesive fracture.

The examination of these two mechanisms has been conducted in the context of flexural and extensional modes. It has been shown that, in flexural modes, tensile stresses initiates fractures which is subsequently followed by cohesive and adhesive fractures [18], [19], whereas the second mechanism has been reported for extensional modes at high frequencies (32 kHz) [20], [21].

This contribution concentrates on the second mechanism of deicing using extensional modes.

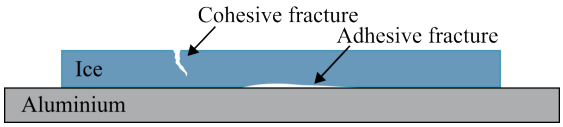

Fig. 2 Cohesive and adhesive fracture illustration.

1.2. Finite element analyses

A modal analysis is conducted to determine the natural frequencies, mode shapes, and shear stress levels on the surface of the substrate. An aluminum alloy A5 1050 plate (150 mm × 50 mm × 1.5 mm) with one round hard PZT (PIC181) piezoelectric ceramic (ø 20 mm, 1 mm) bonded underneath in the center, was modeled numerically in 3D using the finite element software COMSOL (Fig. 3). The sample is held in free boundary conditions. The round shape of piezoelectric ceramic

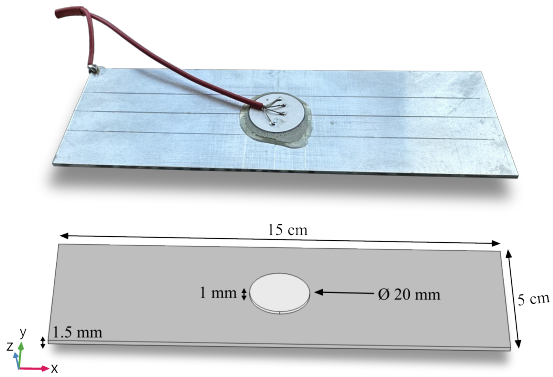

Fig. 3 3D finite element modeling and reel image of the plate.

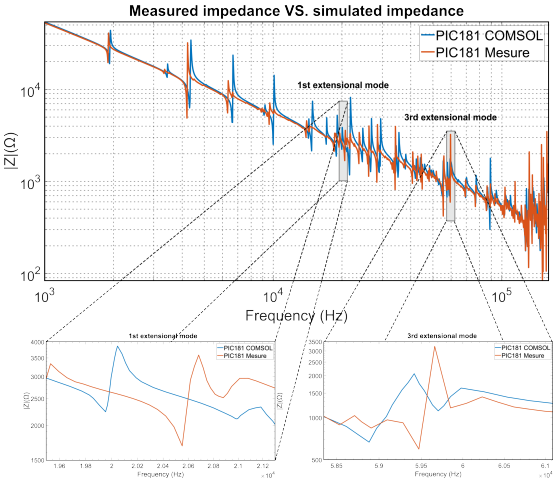

Fig. 4 Measured impedance vs. simulated impedance of the structure (plate + piezoelectric ceramic)

was chosen since it suffers less stress on the edges than a rectangular shape (any shape with angles) [22]. Since we are interested in the second fracture mechanism triggered by extensional modes, the latter is only being studied and tested.

In this case where the actuator is placed in the middle of the plate, only the fundamental extension mode and its odd harmonics will appear in the plate.

According to computations when filtering all modes except extensional one, the first extensional mode (fundamental) is found around 20 kHz (Fig. 5).

However, when the displacement is set to be free on the three axes, the extensional mode will be coupled with flexural modes and other parasitic modes, making it difficult to be observable around 20 kHz (Fig. 6). At the first extensional mode coupled with other modes, stress levels (shear + tensile) were not sufficient for cracking or debonding the 2 mm glaze ice layer and nothing happened experimentally. On the other hand, at the 3rd extensional mode around 60 kHz (Fig. 7 and Fig. 8), stress level (mainly shear stress) was higher, leading to some cohesive fractures but mainly adhesive fractures as illustrated in Fig. 9. In order to amplify the 3rd extensional mode, two other ceramics were bonded to the plate at the extensional wave crests.

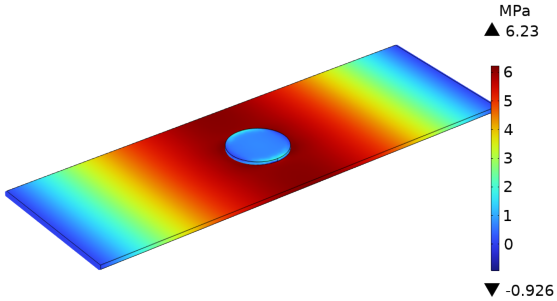

Fig. 5 Shear stress level at the 1st extension mode at 20 kHz with zero displacement imposed on the y and z axes.

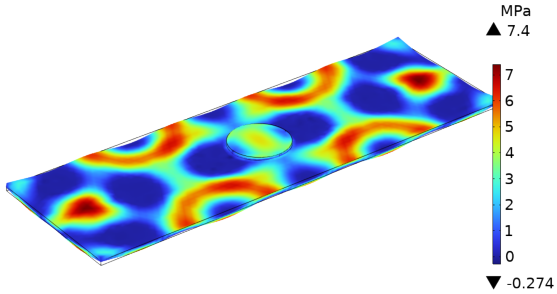

Fig. 6 Stress level at the 1st extension mode around 20 kHz with free displacement on the x, y and z axes.

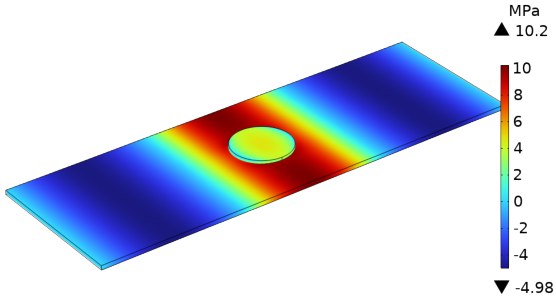

Fig. 7 Shear stress level at the 3rd extension mode at 59 kHz with zero displacement imposed on the y and z axes.

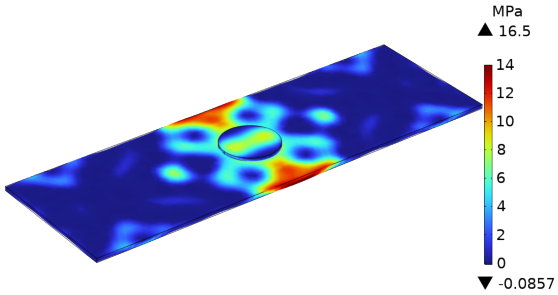

Fig. 8 Shear stress level at the 3rd extension mode at 59 kHz with zero displacement imposed on the y and z axes.

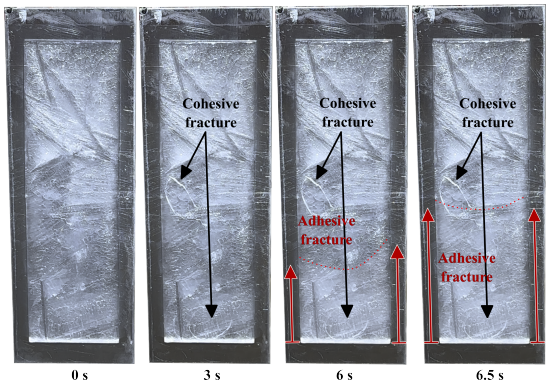

Fig. 9 Cohesive fractures and propagation of adhesive fracture at the 3rd extension mode.

Simulation results show as expected, a shear stress level approximately three times higher for the 3rd mode compared to when only one actuator is used (Fig. 10). in experimental tests for the 3rd mode, we observe initial cohesive fractures due to parasitic modes, followed by adhesive fractures, and then a complete debonding of the ice. These three stages occur almost instantaneously at 200 V, taking place within a span of approximately 5 seconds as illustrated in Fig. 13.

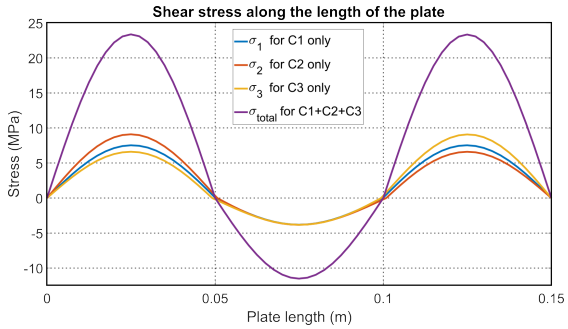

Fig. 10 Shear stress level traced along a line that runs the length of the plate at the 3rd extension mode for one actuator at a time, and then all three together.

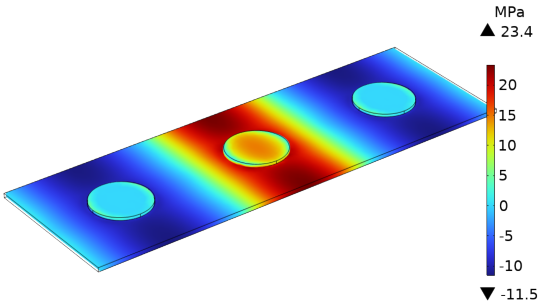

Fig. 11 Shear stress level at the 3rd extension mode at 59 kHz with zero displacement imposed on the y and z axes.

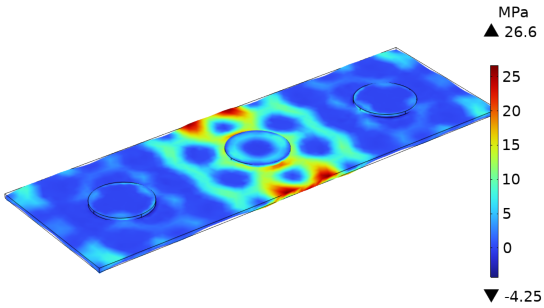

Fig. 12 Shear stress level at the 3rd extension mode around 59 kHz with free displacement on the x, y and z axes.

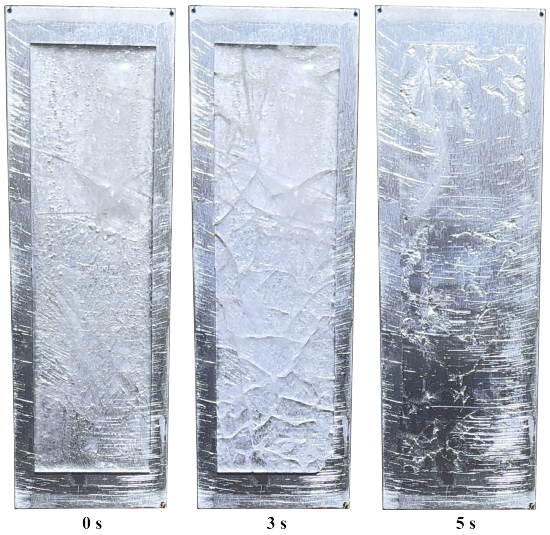

Fig. 13 Experimental result of deicing a 2 mm glaze ice layer at the 3rd extension mode of the rectangular plate.

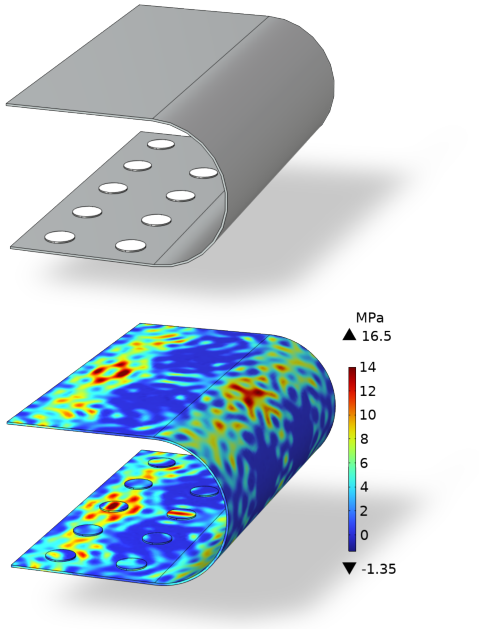

Fig. 14 Computation result of the 7th extension mode.

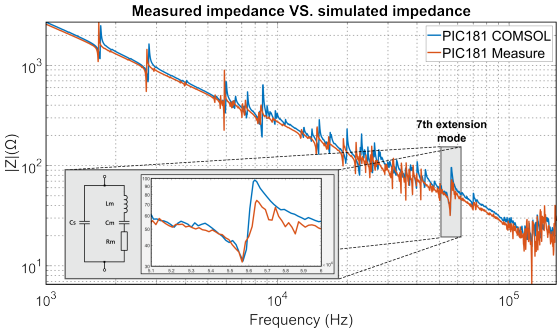

Fig. 15 Van Dyke circuit model of the setup in Fig. 14 around the 7th extension mode.

Once the numerical model of the small plate is validated, a more representative model was made. A large curved plate of aluminum of 350 mm × 250 mm × 1.5 mm dimension with 20 actuators with the same dimensions and material as used previously were employed to create the finale setup. The same strategy was used for driving and placing the actuators. As illustrated in Fig. 14, actuators were placed in a way to amplify the 7th extension mode at 55 kHz (Fig. 15) where we get enough stress and thus enough displacement to crack and delaminate the ice.

2. Electrical specifications of the whole system

In order to properly drive a piezoelectric actuator and improve its performance, it is essential to know its electrical characteristics. The equivalent electrical model of a piezoelectric actuator presents a highly capacitive load (C_s) related to its dielectric behavior, along with a parallel motional branch (L_m, C_m, R_m) representing the vibrational behavior of the mechanical part. Each piezoelectric actuator has several resonance frequencies in which its impedance has a lower magnitude as compared to non-resonance frequencies. To attain higher efficiency and deliver more power to the ultrasound system, actuators should be excited at their dominant resonance frequency which corresponds in our case to the 7th extension mode at 55 kHz.

The deicing system and its power supply must comply with the aviation regulations and standards (DO 160), as well as the installation constraints of the equipment (safety, space requirements), while allowing its proper operation.

The power supply should deliver a sinusoidal voltage to the actuators in order to excite the desired mode. Otherwise, undesired harmonics (low-quality signal) can deteriorate the actuator's performance and increase power consumption in the system.

Finally, given the space constraints that do not allow to place the converter to be as close as possible to the load (actuators), the latter will be fed through 2 meters long cables.

3. Investigation on the driving power supply topology

Given that the electrical behavior is influenced by the mechanical load and temperature [22], it becomes crucial to take certain factors into account when designing the power supply. One is the driving frequency which must correspond to the mechanical resonance frequency of the actuators attached to the leading edge. In fact, at this resonance, the power transfer is better, and the reactive energy consumption is reduced (fewer losses). Another important factor is the quality of the excitation signal, which significantly influences the performance and lifetime of the piezoelectric actuators [23].

In this regard, various literature has focused on driving piezoelectric actuators using voltage source inverters. Resonant inverters (LC or LLCC) and PWM inverters (LC or LLCC) are the most commonly used. Other topologies have been used, such as the three-level

NPC inverter and the current inverter. The main disadvantages of resonant inverters are the volume and weight of the magnetic elements of the resonant filter and a very limited variation of the operating frequency. To overcome these drawbacks, PWM-controlled inverters (LC or LLCC) have been proposed [24]. The disadvantages of PWM control are often related to the switching frequency, which generates high switching losses and EMC (Electromagnetic Compatibility) problems. These issues can be particularly limiting in some cases, especially when GaN transistors are employed.

In [22], an investigation of three interesting topologies for driving ultrasound piezoelectric actuators under aeronautical constraints was conducted. The study revealed the predominance of the ARCPI (Auxiliary Resonant Commutated Pole Inverter) structure over the current source inverter (CSI) and the Energy Recovery "Resonant" structure.

Auxiliary Resonant Commutated Pole Inverter (ARCPI)

The inverter consists of two main arms and an auxiliary circuit connected to a capacitive divider bridge (Fig. 16). In order to limit losses as well as the number of components, one arm is switched at Low Frequency (LF) synchronized to the transducer frequency, and the other is switched at High Frequency (HF), on which the auxiliary circuit is connected. The role of this circuit is to charge and discharge the parasitic capacitances C_{oss} to ensure ZVS condition on the HF arm. On the other hand, the control law of the auxiliary circuit implies zero current switching (ZCS) of its transistors. Moreover, since the auxiliary circuit is not in the main power path, the power rating of its switches will be reduced compared to that of the main switches. The control applied is a unipolar PWM which reduces the output voltage harmonics.

The laboratory setup for the ARCPI converter is depicted in Fig. 17. To ensure high precision in the driving frequency, the converter's control was implemented in an FPGA. The LF arm operates at low frequency (55 kHz) synchronized to the output voltage while the HF arm is switched at high frequency at 2 MHz, under 270 Vdc bus voltage.

The curved setup (Fig. 14) was tested at the 7th extension mode at 55 kHz using the ARCPI converter. At this frequency, an instantaneous cracking and delamination of 2 mm-thick-ice occurred with power input density of 0.074 W/cm² and a ratio of 0.07

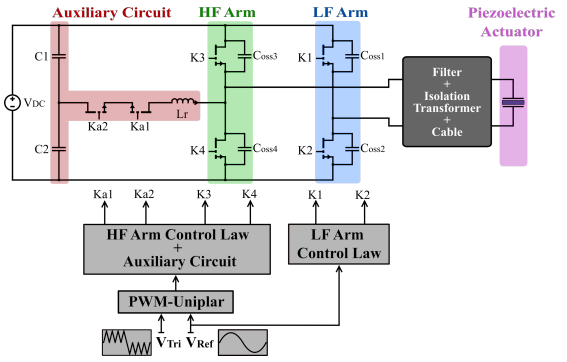

Fig. 16 Experimental setup of the complete deicing system.

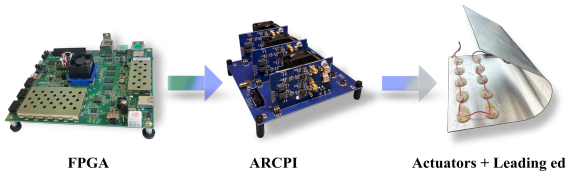

Fig. 17 Circuit topology of the ARCP Inverter.

piezoelectric actuators per cm². However, the driving power converter should be sized to deliver at least 356 VA to the actuators due to their capacitive behavior and the voltage level needed to initiate fractures in the ice.

Conclusion

The concept of deicing based on extensional modes using piezoelectric actuators was demonstrated.

COMSOL finite element simulations were used to determine the proper excitation mode and the positioning of piezoelectric actuators.

A converter topology was carefully selected and developed in the laboratory, through which, an adequate amount of power was delivered to ensure deicing. Experimental results showed complete deicing with a power input density of 0.074 W/cm² and a ratio of 0.07 piezoelectric actuator par cm².

References

[1] « Aviation Maintenance Technician Handbook - Airframe Volume 2 », p. 564.

[2] Robert D. Goehner, Norman I. Glover, et Donald G. Hensley, « ELECTRO-IMPULSE DE-CING SYSTEM FOR AIRCRAFT », 4,678,144, 7 juillet 1987

[3] Richard Alexander Olson et Mark Ronald Bridgeford, « ELECTRO-EXPULSIVE DE-CING SYSTEM FOR AIRCRAFT AND OTHER APPLICATIONS », US 2010/0288882 A1, 18 novembre 2010

[4] P. GONIDEC, J. RAMI, H. MAALIOUNE, R. BILLARD, V. RIGOLET, et J.-D. SAUZADE, « Methode for supplying electric power to a nacelle defrosting system and ice protection

system through ultrasound », WO 2019/180361 A1, 26 septembre 2019
[5] M. Budinger, V. Pommier-Budinger, A. Reysset, et V. Palanque, « Electromechanical Resonant Ice Protection Systems: Energetic and Power Considerations », AIAA J., vol. 59, no 7, p. 2590-2602, juill. 2021, doi: 10.2514/1.J060008.
[6] M. Budinger, V. Pommier-Budinger, G. Napias, et A. Costa da Silva, « Ultrasonic Ice Protection Systems: Analytical and Numerical Models for Architecture Tradeoff », J. Aircr., vol. 53, no 3, p. 680-690, mai 2016, doi: 10.2514/1.C033625.
[7] S. Struggl, J. Korak, et C. Feyrer, « A basic approach for wing leading deicing by smart structures », présenté à SPIE Smart Structures and Materials + Nondestructive Evaluation and Health Monitoring, M. Tomizuka, Éd., San Diego, California, USA, mars 2011, p. 79815L. doi: 10.1117/12.880470.
[8] A. M. A. Mohamed et M. Farzaneh, « An experimental study on the tensile properties of atmospheric ice », Cold Reg. Sci. Technol., vol. 68, no 3, p. 91-98, sept. 2011, doi: 10.1016/j.coldregions.2011.06.012.
[9] S. R. J. et C. M. L., « Structural properties of impact ices accreted on aircraft structures.pdf ». 1 janvier 1987.
[10] P. H. Gammon, H. Kiefte, M. J. Clouter, et W. W. Denner, « Elastic Constants of Artificial and Natural Ice Samples by Brillouin Spectroscopy », J. Glaciol., vol. 29, no 103, p. 433-460, 1983, doi: 10.3189/S0022143000030355.
[11] U. Nakaya, « Visco-elastic Properties of Snow and Ice in Greenland Ice Cap ».
[12] J. Druez, C. L. Phan, J. L. Laforte, et D. D. Nguyen, « The Adhesion of Glaze and Rime on Aluminium Electrical Conductors », Trans. Can. Soc. Mech. Eng., vol. 5, no 4, p. 215-220, déc. 1978, doi: 10.1139/tcsme-1978-0033.
[13] J. J. Petrovic, « Review Mechanical properties of ice and snow ».
[14] « The adhesion and strength properties of ice », Proc. R. Soc. Lond. Ser. Math. Phys. Sci., vol. 245, no 1241, p. 184-201, juin 1958, doi: 10.1098/rspa.1958.0076.
[15] C. Laforte et J.-L. Laforte, « Deicing Strains and Stresses of Iced Substrates », J. Adhes. Sci. Technol., vol. 26, no 4-5, p. 603-620, mars 2012, doi: 10.1163/016942411X574790.
[16] F. Guerin, C. Laforte, M.-I. Farinas, et J. Perron, « Analytical model based on experimental data of centrifuge ice adhesion tests with different substrates », Cold Reg. Sci. Technol., vol. 121, p. 93-99, janv. 2016, doi: 10.1016/j.coldregions.2015.10.011.
[17] H. H. G. JeUinek, « ADHESIVE PROPERTIES OF ICE ».
[18] M. Budinger, V. Pommier-Budinger, L. Bennani, P. Rouset, E. Bonaccurso, et F. Dezitter, « Electromechanical Resonant Ice Protection Systems: Analysis of Fracture Propagation Mechanisms », AIAA J., vol. 56, no 11, p. 4412-4422, nov. 2018, doi: 10.2514/1.J056663.
[19] E. Villeneuve, C. Volat, et S. Ghinet, « Numerical and Experimental Investigation of the Design of a Piezoelectric De-Icing System for Small Rotorcraft Part 1/3: Development of a Flat Plate Numerical Model with Experimental Validation », Aerospace, vol. 7, no 5, p. 62, mai 2020, doi: 10.3390/aerospace7050062.
[20] J. L. Palacios et E. C. Smith, « Investigation of an Ultrasonic Ice Protection System for Helicopter Rotor Blades ».
[21] J. Palacios, E. Smith, J. Rose, et R. Royer, « Ultrasonic De-Icing of Wind-Tunnel Impact Icing », J. Aircr., vol. 48, no 3, p. 1020-1027, mai 2011, doi: 10.2514/1.C031201.
[22] M. Jomaa, D. Vasic, F. Costa, P.-E. Levy, et M. Ali, « Driving power supply for an avionic piezoelectric deicing system », in Active and Passive Smart Structures and Integrated Systems XVII, S. Tol, M. A. Nouh, S. Shahab, J. Yang, et G. Huang, Éd., Long Beach, United States: SPIE, avr. 2023, p. 90. doi: 10.1117/12.2657036.
[23] Rongyuan Li, N. Frohleke, et J. Bocker, « LLCC-PWM inverter for driving high-power piezoelectric actuators », in *2008 13th International Power Electronics and Motion Control Conference*, Poznan, Poland: IEEE, sept. 2008, p. 159-164. doi: 10.1109/EPEPEMC.2008.4635261.
[24] C. Kauczor et N. Frohleke, « Inverter topologies for ultrasonic piezoelectric transducers with high mechanical Q-factor », in *2004 IEEE 35th Annual Power Electronics Specialists Conference (IEEE Cat. No.04CH37551)*, Aachen, Germany: IEEE, 2004, p. 2736-2741. doi: 10.1109/PESC.2004.1355265.